frontiers | Frontiers in Earth Science

ORIGINAL RESEARCH
published: 06 July 2022
doi: 10.3389/feart.2022.900314

The Influences of Climatic and Lithological Factors on Weathering of Sediments in Humid Badland Areas

Chunxia Xie[1], Nevena Antić[2], Estela Nadal-Romero[3], Luobin Yan[4], Tomislav Tosti[5], Svetlana Djogo Mračević[6], Xinjun Tu[1] and Milica Kašanin-Grubin[2]**

[1]School of Geography and Planning, and Center of Water Resources and Environment, Sun Yat-sen University, Guangzhou, China, [2]Department of Chemistry, Institute of Chemistry, Technology and Metallurgy, University of Belgrade, Belgrade, Serbia, [3]Instituto Pirenaico de Ecología, Procesos Geoambientales y Cambio Global, IPE-CSIC, Zaragoza, Spain, [4]School of Geographical Sciences, Southwest University, Chongqing, China, [5]Faculty of Chemistry, University of Belgrade, Belgrade, Serbia, [6]Faculty of Pharmacy, University of Belgrade, Belgrade, Serbia

OPEN ACCESS

Edited by:
Waldemar Kociuba, Maria Curie-Sklodowska University, Poland

Reviewed by:
Zdzisław Jary, University of Wrocław, Poland
Przemyslaw Mroczek, Marie Curie-Sklodowska University, Poland

***Correspondence:**
Xinjun Tu
eestxj@mail.sysu.edu.cn
Milica Kašanin-Grubin
svetlana.djogo@pharmacy.bg.ac.rs

Specialty section:
This article was submitted to Quaternary Science, Geomorphology and Paleoenvironment, a section of the journal Frontiers in Earth Science

Received: *20 March 2022*
Accepted: *19 May 2022*
Published: *06 July 2022*

Citation:
Xie C, Antić N, Nadal-Romero E, Yan L, Tosti T, Djogo Mračević S, Tu X and Kašanin-Grubin M (2022) The Influences of Climatic and Lithological Factors on Weathering of Sediments in Humid Badland Areas. Front. Earth Sci. 10:900314. doi: 10.3389/feart.2022.900314

Climate variables including temperature, rainfall intensity, rainfall acidity, and lithological properties are among the most important factors affecting rock weathering. However, the relative contribution of these four factors on rock weathering, especially on chemical weathering, is still unclear. In this study, we carried out a series of weathering-leaching rainfall simulations on four types of badland sediments under controlled conditions of two levels of temperature, rainfall intensity, and rainfall acidity based on the real field data from representative weather scenarios. The main objectives are 1) to explore the progressive change of sample surface and leachate characteristics and 2) to reveal the independent effects of temperature, rainfall intensity, rainfall acidity, and lithology and their relative contribution as well, on both mechanical and chemical weathering. Qualitative analysis on crack development and fragmentation of sample surface and quantitative analysis on the leachate volume, pH, electrical conductivity, and total cation and anion releases of sample leachate together demonstrated that for the investigated sediments, under the conditions of temperature, intensity, and acidity of rain that can be achieved in nature, high drying temperature obviously increases mechanical disintegration by promoting the rate and magnitude of moisture variations (wetting–drying alterations), while high rainfall intensity and acid rain have no obvious effect. Impact and importance of the drying process caused by high temperature between wetting events need more attention, rather than high rainfall intensity. Low temperature, high rainfall intensity, and acid rain contributing more hydrogen ions required for cation exchanges, rock type with more soluble minerals, all promote chemical weathering, and the influence of climatic and lithological factors on chemical weathering decreases in the following order: mineral composition > rainfall intensity > temperature > rainfall acidity. Climatic variations on temperature can modify weathering processes and in that way conditioned hydro-geomorphological processes in badland areas. Such changes should be considered for direct and indirect implications on badland dynamics.

Keywords: badlands, weathering, temperature, rainfall intensity, rainfall acidity, total ion release

1 INTRODUCTION

Weathering processes, which involve mechanical disintegration and chemical decomposition, are a fundamental part of the geological cycle that should be regarded as equally important as erosion, diagenesis, metamorphism, and volcanism (Wilson, 2004). Having an essential part in shaping landscapes (Turkington and Paradise, 2005; Migoń, 2013; Viles, 2013), these processes are a starting point of most morphodynamic processes on the Earth surface, which could further cause engineering geological and environmental problems (Chigira and Oyama, 2000).

A significant connection exists between climate variables and both mechanical and chemical weathering (White and Blum, 1995; Egli et al., 2003, 2008; Viles, 2013). In warmer and wetter environments, all other variables being equal, rocks experience faster chemical weathering, while dry cold weather induces mechanical disintegration (Goudie and Viles, 2012). In the abovementioned context, studying rock weathering in differing climates has gained great importance, not only to guide geotechnical engineering, geohazard prevention and control but also to improve the understanding of the effects of global climate change on geomorphic evolution.

Each of the climate variables, such as average temperature, precipitation, and insolation, has a distinct role in weathering of rocks. Temperature is one of the major controlling factors in rock decay through its effect of mechanical and chemical weathering processes (Warke and Smith, 1998; Yan et al., 2018). Temperature operates indirectly through its control on the variations of water content (Yamaguchi et al., 1988; Weiss et al., 2004). Many research studies revealed that temperature differences between freezing and thawing range significantly promote rock decay (Hall, 2007; Zhang et al., 2013; Ghobadi and Torabi-Kaveh, 2014). The number of wetting–drying cycles has a significant influence on rock decay (Cantón et al., 2001; Yan et al., 2018). Zhang et al. (2015) performed a quantitative analysis on the mass loss of purple mudstone and proposed that the disintegration rate of purple mudstone has a power function relationship with temperature and an exponential relationship with temperature gradient. Also, the dissolution rate of primary minerals increases with increasing temperature (White and Blum, 1995).

Regüés et al. (2000) indicated that the energy generated by drying is almost one order of magnitude higher than the ice-growing energy, and consequently water retention energy is not promoting weathering. Drying process caused by high temperature between wetting events intensifies physical disintegration (Cantón et al., 2001) by producing strong thermal stress which increases rock breakdown (Hall and Hall, 1991; Hale and Shakoor, 2003; Aly et al., 2015) and promotes water–gas phase transformation generating stress formation through volume increase (Hale and Shakoor, 2003). Colback and Wiid (1965) also demonstrated that changes in the relative humidity or partial pressure of water in the pores can lower rock strength dramatically, while Wang et al. (2019b) indicated that water absorption and dehydration alter rock structures and affect mechanical properties due to variation of water content altering bonding strength between particles.

Climate change and occurrence of acid rain are distinct but very interrelated processes. With the recent rapid development of industrial and agricultural activities, acid deposition with SO_x and NO_x being emitted is likely to worsen (Vet et al., 2014), which requires a better understanding of the influence of pH on water–rock interaction. The sensitivity of soils and rocks to the impact of acid rain mostly depends on mineralogical composition (Wilson, 2004). If the soil contains a small amount of minerals prone to weathering, then released base cations cannot neutralize the incoming acid deposition; however, if the soil is rich in weatherable base minerals it will be able to effectively neutralize the incoming acidity (Sverdup and Warfynige, 1990). In general, weathering rates of rocks rich in calcium (or magnesium) carbonate are increased due to acid deposition, whereas rocks rich in quartz and muscovite are independent of the pH of the fluid (Gupta and Ahmed, 2007).

Previous studies on the influences of temperature, water supply, water acidity, and lithology on rock weathering were conducted both in the field and laboratory conditions (Likens et al., 1996; Cantón et al., 2001; Kansanin-Grubin and Bryan, 2007; Kansanin-Grubin, 2013; Pulice et al., 2013; Zhang et al., 2015, 2016; Zhao et al., 2018). Field weathering studies were mainly based on on-site monitoring with different weathering processes active at one location and more than one factor playing an important role. Therefore, it is difficult to determine the effect of a certain weathering process or a single factor on the sediment weathering (Bruthans et al., 2017). To minimize the number of variables and isolate the various mechanisms influencing natural weathering, laboratory experiments mostly considered the influence of temperature, water supply, water acidity, or lithology independently (Kansanin-Grubin, 2013; Zhang et al., 2015, 2016; Yan et al., 2018; Zhao et al., 2018), or at most two factors are considered simultaneously (Gupta and Ahmed, 2007; Zhang et al., 2013) under controlled conditions.

Zhang et al. (2013) conducted laboratory wetting–drying and freezing–thawing experiments comparing the effect of water variation and temperature alternation and found that variation of water content and H_2O phase (vapor–liquid–solid) within rock, rather than temperature alternation, is playing a key role in the rock decay processes. Hale and Shakoor (2003) and Erguler and Shakoor (2009) quantified the simultaneous effects of heating–cooling, wetting–drying, and freezing–thawing and found that freezing–thawing process is most effective in causing rock decay. Yan et al. (2018) found that the wetting–drying treatments with temperature differences were more efficient in weathering than wetting–drying treatments without temperature differences. However, the main focus of these studies was on the impact of water–rock interaction on fragmentation (Erguler and Shakoor, 2009; Zhang et al., 2013) and unconfined compressive strength (Hale and Shakoor, 2003), and chemical weathering in these studies received less attention.

Likewise, lithology is one of the factors that affects weathering rate (Lashkaripour and Boomeri, 2002; Piccarreta et al., 2006; Summa et al., 2007). Disintegration rate could be correlated to the pore structure parameters. Sediments with clay minerals as main constituents and pore structure dominated by mesopores (2 ~ 50 nm) have a large specific surface area which is positively

related to water absorption (Lu et al., 2015; Wang et al., 2019a, 2019b). Pore size distribution of mudstones is primarily controlled by grain size, and generally, pore size and permeability decrease as grain size decreases (Yang and Aplin, 2010). However, the same authors indicate that although the relationship between permeability and porosity is never simple, it depends on the clay content, and the lower the clay content, the higher the permeability at the same porosity. Li et al. (2011) found that the significant loss of strength is closely related to water absorption and suggested that the effect of water on the structure of rock pores is one of the major factors which leads to a significant reduction in mechanical rock properties. Also, Li et al. (2019) explained the above link between water absorption and rock strength by the micro-mechanical model that, the increasing absorbed water causes the decrease of attractive force of mineral grains and the increase in the force acting between mineral grains and the pore water. The process of evaporation from porous rock also plays an important role in weathering processes (Slavík et al., 2020), as the rate of evaporation determines the rate and magnitude of moisture variations under a given temperature and moisture input condition. The strong link between porosity character and rock deterioration has also been revealed by many other research studies (Heap et al., 2014; Ondrášik and Kopecký, 2014; Bubeck et al., 2017).

The purpose of this study is to investigate the independent and interactive effects of drying temperatures, rainfall intensity, rainfall acidity, and lithology on the weathering rate of highly erodible badland sediments. To accomplish this purpose, four types of badland sediments collected from similar humid badland areas, three from China and one from Spain, were selected. Gallart et al. (2002) identified three homogeneous groups of badland types as a function of their climate distribution, general characteristics, and dominant processes. Humid badlands are the group of badlands with annual precipitation exceeding 700 m, and where the dominant weathering processes include freezing–thawing and wetting–drying cycles. Compared to badlands in arid or semi-arid areas, humid badlands are subject to higher denudation rates and dynamics and suffer from rapid and intense weathering (Gallart et al., 2002; Gallart et al., 2013; Nadal-Romero et al., 2015). A series of weathering experiments under controlled conditions combined of different temperatures, rainfall intensities, and rainfall acidities based on real field data from representative weather scenarios were conducted to explore progressive change of sample surface and leachate characteristics. With this study, we hypothesize that the drying temperature has a crucial role in sediment disintegration. Additionally, we want to test whether the chemical weathering is occurring also in sediments that are not primarily built of dissolvable minerals.

2 MATERIALS AND METHODS

2.1 Badland Sites and Sampling

Four badland sites were selected to assure a variety of sediments with different lithologies: Datang badlands, Jiangtian badlands, and Xiahui badlands in China, developed in Cretaceous-Eocene red bed mudstones of Nongshan Formation (En), Shanghu Formation (Esh), and Zhutian formation (Kzt), respectively; and Araguás badlands in Spain, developed in the Eocene marl formation. The climate in these four badland sites is similar humid (precipitation > 700 mm), all characterized by strong seasonal contrasts in both rainfall and temperature distribution, and weathering processes of badlands under these climatic conditions include both wetting–thawing and freezing–thawing cycles (Nadal-Romero and Regüés, 2010; Yan et al., 2018; Chen et al., 2021).

Three badland areas, Datang (25°17′6″N, 114°30′59″E), Jiangtian (25°15′38″N, 114°32′17″E), and Xiahui (25°16′19″N, 114°30′2″E), are all located in Nanxiong Basin, southeast of China (**Figures 1A**, **2A**). A subtropical monsoon humid climate prevails, with four distinct seasons, hot rainy summers and cold mostly dry winters. According to the meteorological data (1980–2020), the average annual temperature is ~20°C, with a maximum of 34°C during the summer and a minimum of 6°C during the winter; the average number of freezing day is 9.3 days. The average annual precipitation is ~1,500 mm, occurring mostly from April to June.

Araguás badlands (42°35′45″N, 0°37′15″W), located in the Inner Pyrenean Depression, northeast of Spain (**Figures 1B**, **2B**), are developed in the Eocene marl formation. The climate is largely Mediterranean with some continental and Atlantic influences. The average annual precipitation is ~800 mm (1980–2020), with maximums in spring and autumn. The average annual temperature is approximately 10°C, with minimums of −14°C and maximums in excess of 30°C.

Unweathered sediment samples were collected from the four badland sites and marked as the first letters of the badland area name: sample D from the Datang badland, sample J from the Jiangtian badland, sample X from the Xiahui badland, and sample A from the Araguás badland. At all four sites, samples of unweathered material were collected and transferred to the laboratory for further analyses.

2.2 Methodology

2.2.1 Measurements of the Properties of the Parent Material

Mineralogical composition of sediments was determined by X-ray powder diffraction performed on the Philips 1710 PW diffractometer with CuKα 1.2 (1.54178 A°) radiation. X-ray diffraction was recorded over 2–70° interval with a step size of 0.02° and fixed counting time of 1 s per step. Concentrations of major elements were determined using the X-ray Fluorescence (XRF). Before analyses, samples were dried at 105°C until the constant mass was mixed with wax (sediment: wax = 80:20; Hoechst wax C micro powder produced by Merck) and pressed into tablets using 25t pressure for 5 min. Semiquantitative and qualitative analyses were performed using Spectro Xepos Energy Dispersive KSRF (EDXRF).

2.2.2 Weathering Rainfall Simulation Experiment

Rainfall intensity, rainfall acidity, and drying temperature were chosen as climatic variables influencing mechanical and chemical weathering. During the experiment, distilled water was used as a

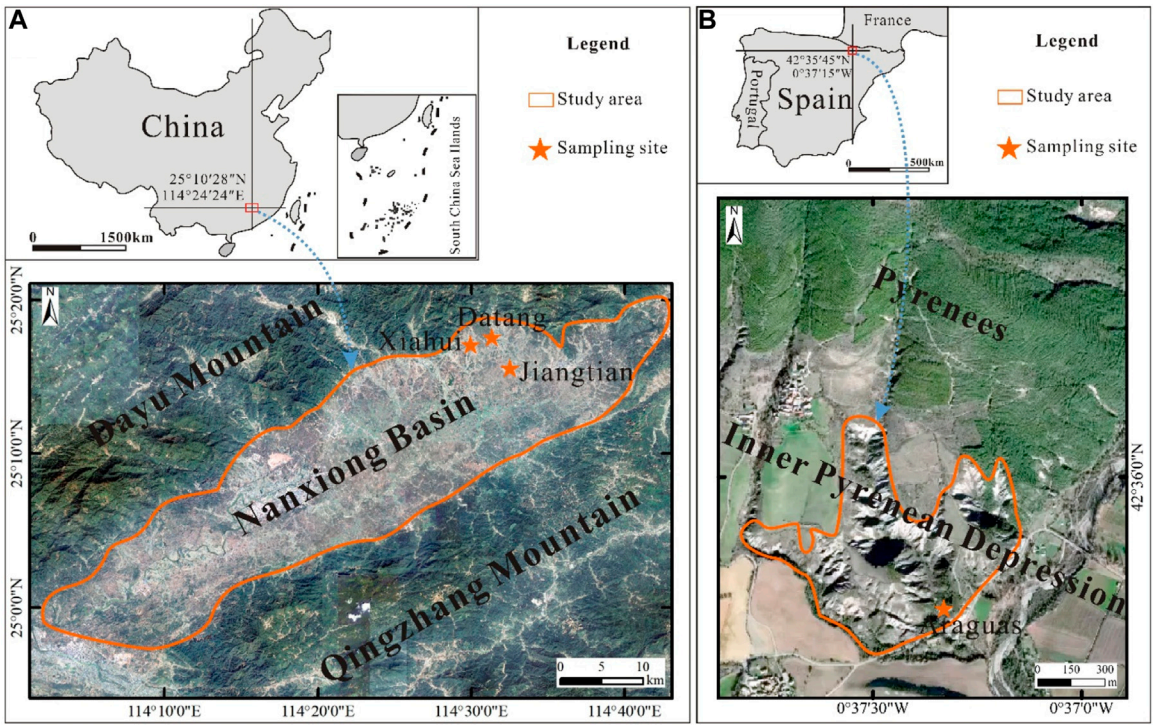

FIGURE 1 | Location of the badland study area and sampling sites in **(A)** Nanxiong Basin (China) and **(B)** Inner Pyrenean Depression (Spain) (Source of satellite image: https://earth.google.com/).

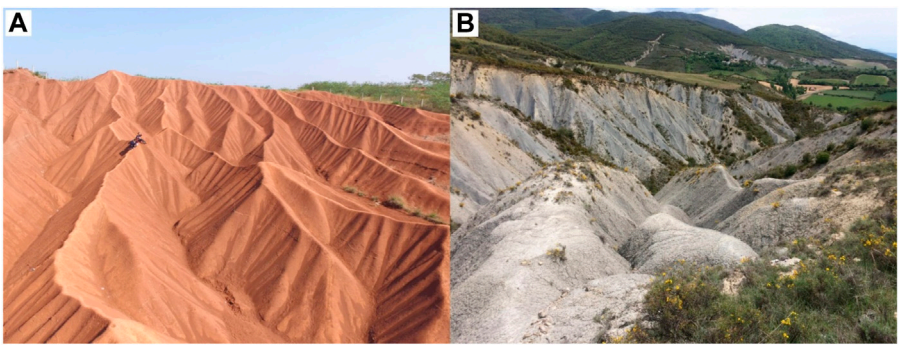

FIGURE 2 | Badland landscapes in **(A)** Nanxiong Basin (China) and **(B)** Inner Pyrenean Depression (Spain).

substitute for natural rain, while acid rain was made in the laboratory by adding acid in the ratio H_2SO_4:HNO_3 = 3:1 until pH ~4.4 was reached. Based on the acid rain monitoring results maintained by Shaoguan Environmental Monitoring Center Station 2005–2014, statistics and analysis showed that the average frequency of acid rain was 61.8%, and the mean pH of acid rain in Shaoguan was 4.42 (Huang and Xie, 2015).

The unweathered shards were placed in circular sample holders with a mesh bottom (10.5 cm × 4.5 cm x 0.5 mm), above funnels that permitted leachate collection. The influence of rainfall intensity was assessed by the comparison between two levels, high-intensity rainfall (H), 15 ml min^{-1}, and low-intensity rainfall, (L) ~4.5 ml min^{-1}. The low-intensity rainfall was obtained in 10 min of water spraying, a total volume of ~48 ml water, while the high-intensity rainfall was obtained in 10 min of water spraying, a total volume of ~148 ml water. Due to the limited amount of samples, low-intensity rainfall was only performed on samples D, J, and X under natural rain. The influence of temperature was assessed by comparing the high-drying temperature of ~50°C (the average maximum surface temperature) (D) and low freezing temperature of −5°C (the extreme minimum surface temperature) (F). The procedures and

TABLE 1 | Explanation of treatments exploring the influence of climatic variables (N—natural rain; A—acid rain; H—high rainfall intensity; L—low rainfall intensity; D—high drying temperature; and F—freezing temperature).

Climatic variable			Treatment code	Representative weather scenarios	Steps
Rainfall acidity	Rainfall intensity	Temperature			
N	H	D	NHD	Heavy rainy days in summer	1. Sample under rainfall of deionized water at 888 ml/h intensity for 10 min 2. Sample in the oven at 53°C for 6 h 3. Sample at the room temperature (18–25°C) for 18 h
N	H	F	NHF	Heavy rainy days in winter	1. Sample under rainfall equipment sprinkling deionized water at 888 ml/h intensity for 10 min 2. Sample in −5°C freezer for 16 h 3. Sample at the room temperature (18–25°C) for 8 h
N	L	D	NLD	Light rainy days in summer	1. Sample under rainfall of deionized water at 288 ml/h intensity for 10 min 2. Sample in the oven at 53°C for 6 h 3. Sample at the room temperature (18–25°C) for 18 h
N	L	F	NLF	Light rainy days in winter	1. Sample under rainfall of deionized water at 288 ml/h intensity for 10 min 2. Sample in −5°C freezer for 16 h 3. Sample at the room temperature (18–25°C) for 8 h
A	H	D	AHD	Heavy acid-rainy days in summer	1. Sample under rainfall of acid solution at 888 ml/h intensity for 10 min 2. Sample in the oven at 53°C for 6 h 3. Sample at the room temperature (18–25°C) for 18 h
A	H	F	AHF	Heavy acid-rainy days in winter	1. Sample under rainfall of acid solution at 888 ml/h intensity for 10 min 2. Sample in −5°C freezer for 16 h 3. Sample at the room temperature (18–25°C) for 8 h

treatment codes are given in **Table 1**. Three steps in the experiment were referred to as a cycle. The surface and leachate characteristics were monitored in each cycle. Fifteen cycles were carried out for each treatment, as the surface changing and ion-leaching of most samples basically stayed stable after that.

2.2.3 Measurements of the Properties of the Leachate

Leachate volume, pH, and electrical conductivity (EC) were measured at room temperature in each cycle using measuring cylinder, pH meter AD 1000 pH/mV & Temperature Meter (Adwa), and Iskra 65967.00 conductometer, respectively.

Concentrations of leachate cations (Ca^{2+}, Mg^{2+}, K^{+}, and Na^{+}) in cycles 1–5 and cycles 7, 9, 12, and 15 were determined using inductively coupled plasma—optical emission spectrometry (ICP-OES) (Thermo Scientific iCAP 6000 ICP-spectrometer, SAD) with autosampler CETAC ASKS-spectrometer, SAD.

Concentrations of leachate anions (CO_3^{2-}, SO_4^{2-}, NO_3^{-}, and PO_4^{3-}) in cycles 1–5 and cycles 7, 9, 12, and 15 were determined using Dionex ICS 3000 (Single Pump (SP), Conductivity Detector (CDS), Eluent Generator (EG), Chromeleon® Chromatography Workstation with Chromeleon 6,7 Chromatography Management Software; Column: IonPac AS15 Analytical, 4 × 250 mm (P/N 053940), IonPac AG15 Guard, 4 × 50 mm (P/N 053942), Eluent: 42 mM potassium hydroxide (KOH) (P/N 058900), Flow rate: 1.0 ml/min, Continuously Regenerating Anion Trap Column (CR-ATC) (P/N 060477), Temperature: 30°C, Injection volume: 10 µl, Detection: Suppressed conductivity, ASRS ULTRA II(4 mm) (P/N 061561), recycle mode).

2.2.4 Calculations and Statistical Analyses

Ion mass concentrations found in the leachate were multiplied by leachate volume corresponding to each cycle to obtain the mass of each ion released during the rainfalls. Mass of each released ion was divided by the mass of the initial sediment and afterward divided by molar mass. In this way, we obtained the amount of each ion released from per unit mass of initial sample, that is, ion release. Ion release is a representation of the amount of ions, and it will not be influenced by dilution effect of the leachate or molar mass of different ions, so it permits direct comparisons between different treatments and rock types, and it is used as an index to measure the weathering rate (Zhao et al., 2018). The ion release of all cations and the ion release of all anions were summed to obtain total cation release (Σ cation) and total anion release (Σ anion), respectively.

For interpretation of parameter results, principal component analysis (PCA) and correlation coefficients were calculated using the SPSS Statistics 20 package.

3 RESULTS AND DISCUSSION

3.1 Characteristics of the Parent Material

Both the mineralogical and elemental compositions show similarities among samples D, J, and X, as well as their

TABLE 2 | Composition of the parent material (%).

Sample	D	J	X	A
Silt	53.69	46.74	59.35	56.70
Clay	43.27	53.26	40.65	43.30
SiO_2	46.29	49.30	52.11	43.42
Al_2O_3	15.89	14.87	15.64	14.51
CaO	9.29	8.90	5.84	19.64
Fe_2O_3	6.14	5.37	5.34	4.56
MgO	3.72	4.22	3.84	4.47
K_2O	3.39	3.29	3.10	2.65
Na_2O	0.40	0.54	0.57	0.51

differences from sample A. The mineralogical compositions of samples D, J, and X and sample A have already been reported by Yan, Li et al. (2019), and Nadal-Romero and Regüés (2010), respectively. In terms of mineralogical composition, samples D, J, and X from Datang, Jiangtian, and Xiahui badlands in China are composed of quartz and clay minerals (illite, kaolinite, and chlorite) with the subordinate presence of calcite and hematite (Yan et al., 2018), while sample A from the Araguás badlands in Spain is composed of carbonates (calcite and dolomite), clay minerals (illite and chlorite), quartz, and gypsum (Nadal-Romero and Regüés, 2010). In terms of elemental composition, the calcium oxide contained in sample A is much higher than that of samples D, J, and X (**Table 2**).

3.2 Surface Characteristics During Weathering Experiment

Regardless of rock type, rainfall intensity, or rainfall acidity, pronounced differences in crack development and fragmentation existed between treatments employing high-drying temperatures of 50°C (treatments AHD, NHD, and NLD, **Figure 3**) and freezing temperatures of −5°C (treatments AHF, NHF, and NLF, **Figure 3**). Under freezing-temperature treatments, only few cracks developed and shards slightly disintegrated after 15 repeated freezing–thawing cycles. On the contrary, samples exposed to high-drying temperature treatments disintegrated rapidly (**Figure 3**). Desiccation cracks emerged after the first rainfall cycle, shards broke apart, and after 15 repeated wetting and temperature drying cycles, large shards were reduced into tiny and flaky pieces of ~1 mm–~2 cm in diameter.

No observable differences between surface characteristics occurred between samples treated with acid rain (pH = 4.4) and natural rain (pH = 5.6), revealing that the mechanical disintegration of investigated samples is not controlled by precipitation composition and that material is built of minerals mostly resistant to chemical weathering.

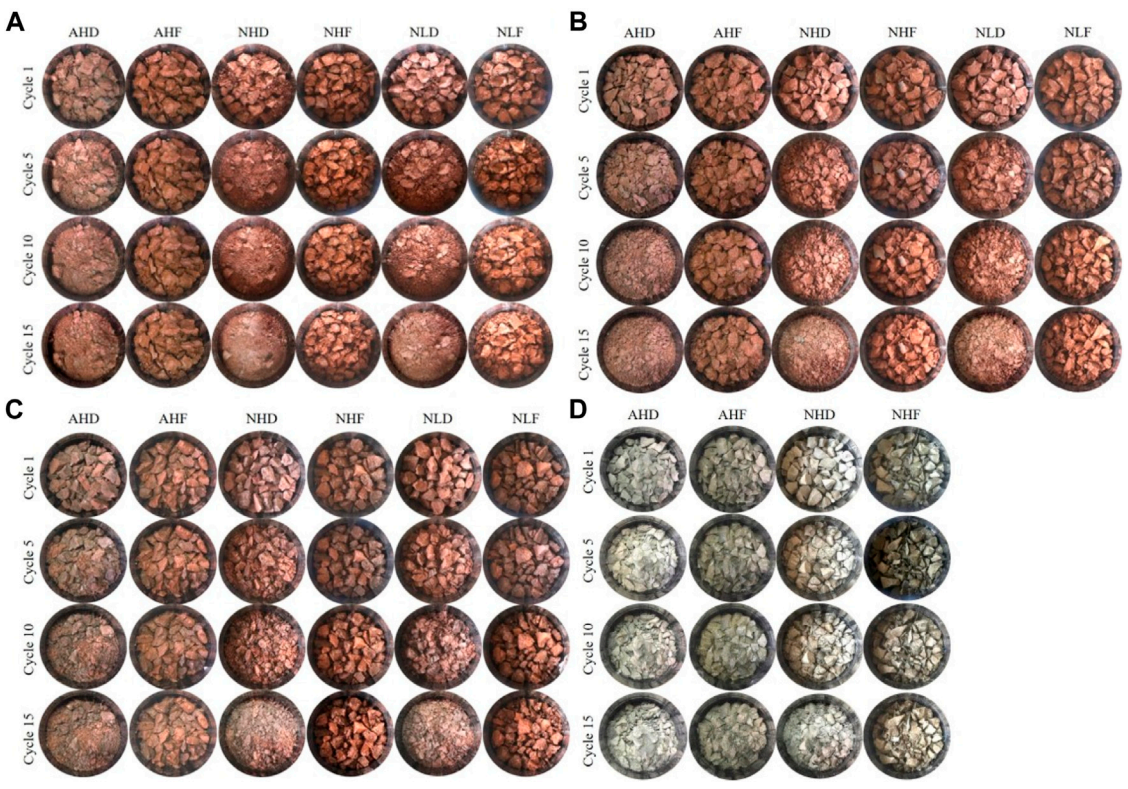

FIGURE 3 | Four types of soft rocks exposed to cycles 1, 5, 10, and 15 of six treatments of different temperatures, rainfall intensities, and acidities. **(A)** D sample from Datang badlands, China; **(B)** J sample from Jiangtian badlands, China; **(C)** X sample from Xiahui badlands, China; **(D)** A sample from Araguás badlands, Spain. Codes of treatments are N—natural rain and A—acid rain; H—high intensity and L—low intensity; D—drying temperature and F—freezing temperature.

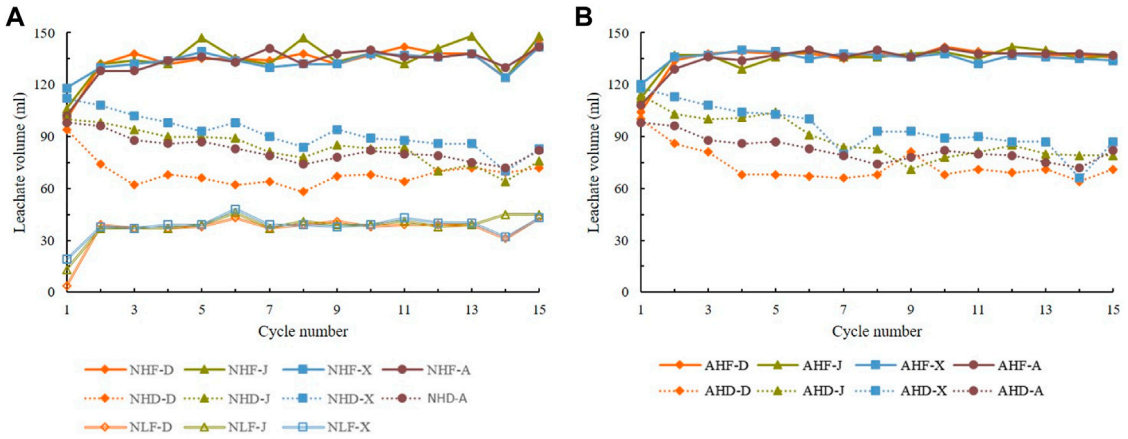

FIGURE 4 | Change of leachate volume over 15 cycles under **(A)** natural rain treatments and **(B)** acid rain treatments. Codes of treatments are N—natural rain and A—acid rain; H—high intensity and L—low intensity, D—drying temperature and F—freezing temperature; D sample from Datang badlands, China; J sample from Jiangtian badlands, China; X sample from Xiahui badlands, China; A sample from Araguás badlands, Spain.

Regardless of the precipitation amount, the freezing–thawing process simulating the winter season causes less visible mechanical disintegration than cycles simulating the hottest days in summer in badlands in both southeast China and Spain. During the latter, cracks of sediment fragments occurred after the first two cycles and a new generation of cracks occurred after every new wetting–drying cycle.

When compared by lithology among the four samples, it can be found that, sample D obviously had a smaller particle size (**Figure 3A**) than the other three (**Figures 3B–D**) during the disintegration processes, which indicates that sample D disintegrates fast among the four.

The progressive appearance of fissures and cracks created a surface regolith composed of tiny shards. Although a compact surface crust was not formed on samples that were under drying treatment, it started to act like one helping in decreasing the leachate volume. Repeated wetting–drying treatments caused large shards to break down into smaller shards due to differential properties of illite and chlorite clay minerals. In addition, the washed-in sediment particles decreased surface porosity (Robinson and Williams, 2000).

3.3 Leachate Characteristics Over Time During Weathering Experiment

Besides the differences in surface characteristics, differences in leachate characteristics caused by treatment conditions and rock types were also evident. During each cycle volume, pH, EC, and ion release were determined in the collected leachate. However, during certain cycles of the low-intensity drying-temperature treatment (NLD), there was not enough leachate produced for the determination of leachate properties. This was the case with cycles 1–15 for D sample, cycles 3–15 for J sample, and cycles 4–15 for X sample.

3.3.1 Leachate Volume

The volume of leachate, highly dependent on both rainfall intensity and temperature, is decreasing in the following order: NHF (AHF) > NHD (AHD) > NLF > NLD (**Figures 4A,B**). Samples that were subjected to low-intensity drying-temperature treatment (NLD) had the lowest leachate volumes, even too low to be measured. Among the samples which produced enough leachate for measurement, samples that received low-intensity rainfall (NLF) had the lowest leachate volumes, very similar for all the three rock types (D, J, and X), with an average of 37 ml (**Figure 4A**).

The leachate volume during the high-intensity rainfall cycles was greatly dependent on drying temperatures regardless of the rainfall acidity (**Figures 4A,B**). Samples that were exposed to freezing temperature (NHF and AHF) produced significantly higher leachate volumes with an average of 135 ml, than samples dried at 50°C (NHD and AHF) with an average of 73 ml. Leachate volumes in all samples under freezing temperature treatments (NHF, AHF, and NLF) increased rapidly between the first two cycles and then tending to be stable in subsequent cycles. Under high-drying temperature treatments, all samples exhibited a general gentle decreasing trend during treatments (NHD and AHD). This is in accordance with the findings of Robison and Philips (2001) who found that infiltration through crusted soil is much slower than through un-crusted. During drying, moisture content is decreasing and the air enters the pores in the sediment. Once the moisture returns, the air pressure builds up and disintegration of sediment fragment occurs (Pejon and Zuquette, 2002).

3.3.2 Leachate pH

Values of pH fluctuating in the range between 7.83 and 9.05 indicate sub-alkaline to alkaline leachate (**Figures 4A,B**). Leachate pH in the high-intensity rainfall treatments (NHD and NHF) is slightly more alkaline than the low-intensity rainfall treatment (NLF) (**Figure 5A**). In acid rain treatments, leachate pH was more alkaline, but without significant differences between samples or treatments (**Figure 5B**).

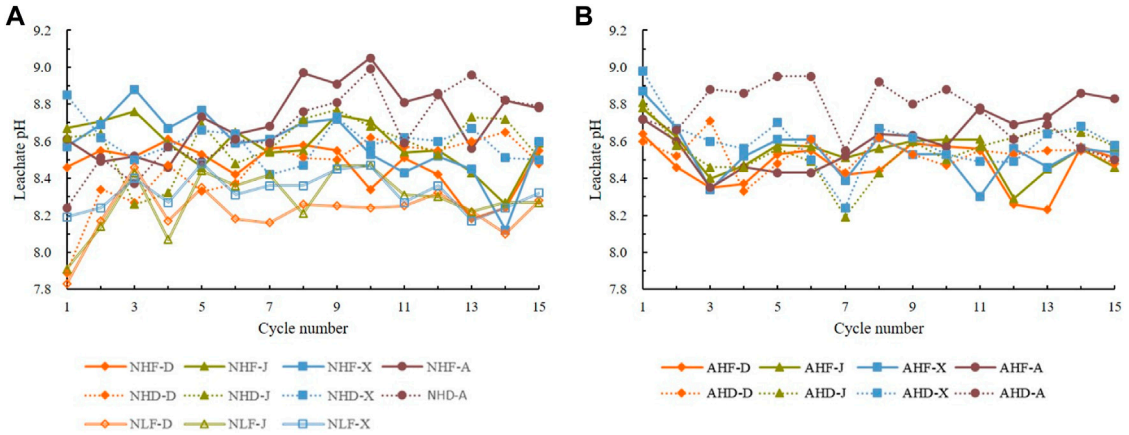

FIGURE 5 | Change of leachate pH over 15 cycles under **(A)** natural rain treatments and **(B)** acid rain treatments. Codes of treatments are N—natural rain and A—acid rain; H—high intensity and L—low intensity; D sample from Datang badlands, China; J sample from Jiangtian badlands, China; X sample from Xiahui badlands, China; A sample from Araguás badlands, Spain.

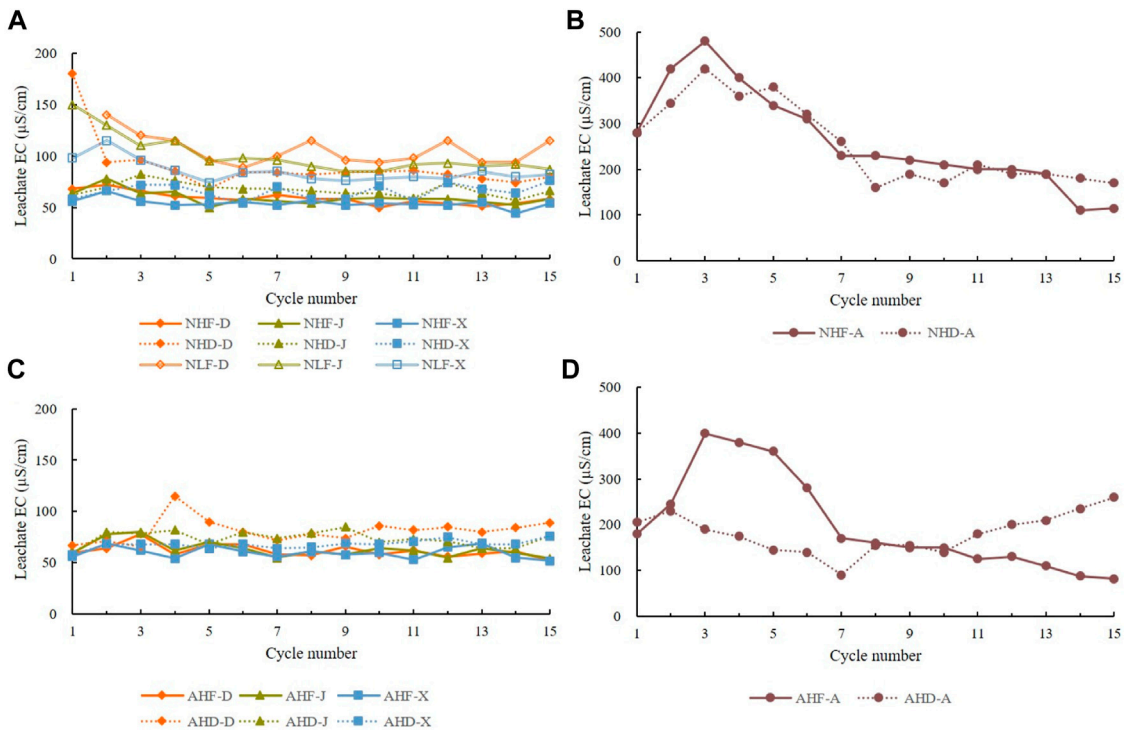

FIGURE 6 | Change of leachate electrical conductivity over 15 cycles. **(A)** D, J, and X under natural rain treatments; **(B)** A under natural treatments; **(C)** D, J, and X under acid rain treatments; **(D)** A under natural treatments. Codes of treatments are N—natural rain and A—acid rain; H—high intensity and L—low intensity; D—drying temperature and F—freezing temperature; D sample from Datang badlands, China; J sample from Jiangtian badlands, China; X sample from Xiahui badlands, China; A sample from Araguás badlands, Spain.

3.3.3 Leachate Electrical Conductivity

Considering all treatments and all samples, EC has a wide range of 44–480 μS/cm (**Figure 6**). Leachate EC showed noticeable differences between sample A from Araguás badlands in Spain and the other three rock types, D, J, and X from badlands in China. Samples D, J, and X had almost the same trend of EC oscillations in the range of 44–180 μS/cm, while the EC of sample A was significantly higher, ranging from 82 to 480 μS/cm, with a sharp peak in the first half of treatment (**Figure 6**). In addition, leachate EC is not significantly affected by treatment type.

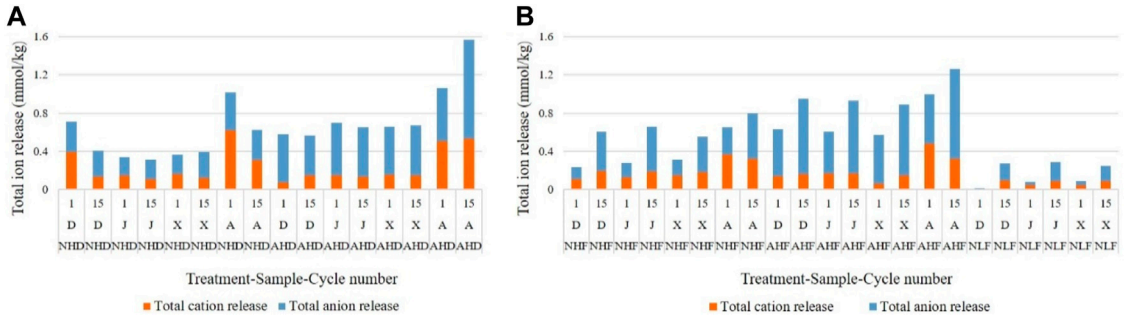

FIGURE 7 | Relation of leached cations and anions under **(A)** drying temperature treatments and **(B)** freezing temperature treatments. Codes of treatments are N—natural rain and A—acid rain; H—high intensity and L—low intensity; D—drying temperature and F—freezing temperature; D sample from Datang badlands, China; J sample from Jiangtian badlands, China; X sample from Xiahui badlands, China; A sample from Araguás badlands, Spain.

In AHF treatment, samples D, X, and J have almost identical trend, while sample A has much higher EC with more drastic oscillations that occur in the first half of treatment and then almost linearly decrease until the end of the experiment.

3.3.4 Ion Release in the Leachate

Ion release in the leachate can give direct insight into chemical processes including hydrolysis and dissolution of minerals during ongoing weathering of sediments. In general, total ion release in the leachate during the experiment was dependent on both rainfall intensity and drying temperature, decreasing in the same order as the leachate volume: NHF (AHF) > NHD (AHD) > NLF > NLD (**Figure 7**).

The individual anion concentration exhibits similar behavior as total ion release. The monovalent anions such as fluoride, bromide, and chloride decrease in first two cycles, with increasing number of cycles there was no evident pattern of behavior. On the other hand, carbonate concentrations decrease with increasing amount of sulfate and vice versa. The obtained results could be explained by the retention mechanism. In the soils, there are two competitive mechanisms based on the electrostatic forces (ion exchange) and size (ion exclusion): If the ion exchange is the dominant mechanism, such as in the beginning of the experiment, the monovalent ions eluted first and their concentrations increase in the leaches; on the other side, in the exclusion chromatography the smallest ions come as the latest. The obtained results lead to conclusion that during drying and freezing processes, the soils change and ion exclusion prevails over ion exchange.

Total cation release showed differences between sample A and samples D, J, and X (**Figure 7**). Samples D, J, and X had lower total cation release in the range of 0.061–0.502 mmol/kg, while sample A had higher total cation release in the range of 0.220–1.241 mmol/kg. Samples D, J, and X leached Ca^{2+} and CO_3^{2-} in the highest concentrations, while sample A, besides these ions, also leached Mg^{2+} and SO_4^{2-} ions. Both the sum of cation (Σ cation) and the sum of anion (Σ anion) have an increasing trend as the weathering progresses in the freezing treatments (**Figure 7B**), while they remain almost constant or even decrease slightly throughout the experiment under the drying temperature (**Figure 7A**).

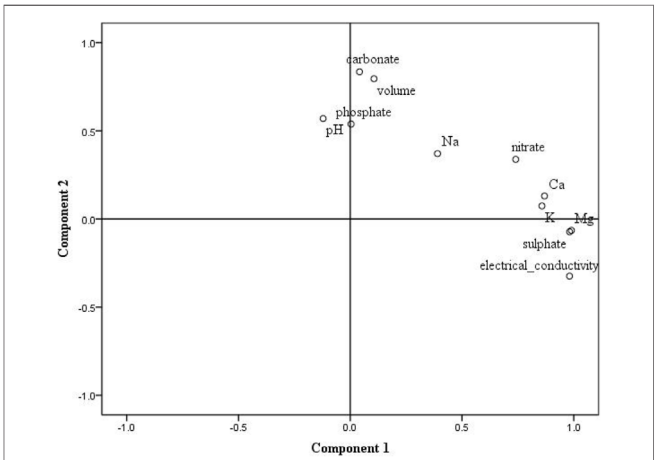

FIGURE 8 | Principal component analyses for leachate properties from sediments from Datang, Jiangtian, and Xiahui badlands, China and Araguás badlands, Spain.

3.4 The Interconnection of Different Leachate Characteristics

Besides comparing the leachate characteristics over time, it is also important to analyze the interconnection of different leachate characteristics to understand the influences that different climate conditions have on sediments and for that purpose the principal component analyses were used. The largest portion of the variables, 68.5%, was concentrated in the first two components. The percentage of variance for the first component is 49.5% which had large positive eigenvector for concentrations of Ca^{2+}, Mg^{2+}, and K^{+}, concentrations of SO_4^{2-} and NO_3^{-}, and electrical conductivity. The percentage of variance of the second component explained 19.0% of variance and it had large positive eigenvector for leachate volume, pH, and concentrations of CO_3^{2-} and PO_4^{3-} (**Figure 8**).

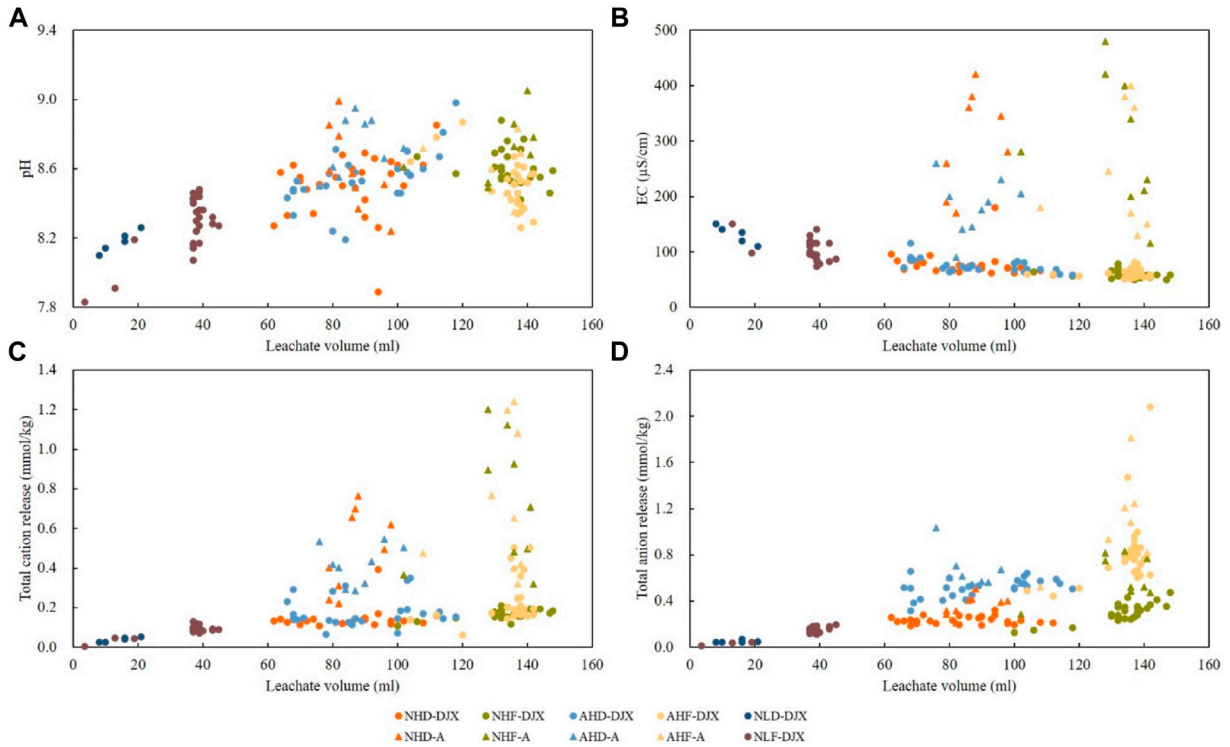

FIGURE 9 | Correlation between **(A)** leachate volume and pH, **(B)** volume and electrical conductivity, **(C)** volume and total cation release, and **(D)** volume and anion release. Codes of treatments are N—natural rain and A—acid rain; H—high intensity and L—low intensity; D—drying temperature and F—freezing temperature; D sample from Datang badlands, China; J sample from Jiangtian badlands, China; X sample from Xiahui badlands, China; A sample from Araguás badlands, Spain.

Better understanding of processes that distinguish different treatments is possible by analyzing correlations between leachate properties. Based on the PCA results, correlation analyses were performed between leachate volume as the parameter explained by the factor 2 and parameters explained by the factor 1, electrical conductivity, total cation, and total anions releases. Additionally, the correlation between leachate volume and pH was analyzed to further explore the influence of acid rain (**Figures 9A–D**). For samples D, J, and X, the correlation coefficients of leachate pH (**Figure 9A**), EC (**Figure 9B**), total cation release (**Figure 9C**), and total anion release (**Figure 9D**) with leachate volume were 0.504, −0.837, 0.757, and 0.725, respectively. For sample A, statistically significant correlation exists only between leachate volume and total cation release (0.407) and total anion release (0.452). As explained above, in the case of this sample a wide range of pH and EC between cycles caused dispersion of results and lack of correlation.

All measured leachate properties depend on both rainfall intensity and temperature: both total cation release and total anion release were decreasing in the same order as the leachate volume was decreasing: NHF (AHF) > NHD (AHD) > NLF > NLD (**Figures 9C,D**), while EC was decreasing in the opposite order: NLD > NLF > NHD (AHD) > NHF (AHF) (**Figure 9B**). With the increase of leachate volume, the leachate alkalinity under high rainfall intensity was significantly higher than under low rainfall intensity regardless of temperature, but there was no significant increase at low freezing temperature compared with high-drying temperature under high rainfall intensity (**Figure 9A**). It is also interesting that acid rain is not significantly influencing the leachate pH in the case of all four tested sediments.

Sediments during the drying treatments are mechanically weathered, and once fragments decrease in size the active surface is increasing. However, there are interactions both on the surface and inside the fragments. Freezing temperature treatments caused significantly higher leachate volume and slightly lower EC than drying temperatures (**Figure 9B**). This could be explained because less evaporation under low temperature increased leachate volume, which enhanced the percolation effect. This indicates that the high-intensity rainfall with freezing promotes chemical weathering rate, although it is not considerable for this type of fine-grained sediments. This is in accordance with findings of Spatti Junior et al. (2019) that chemical weathering of mudstones is more effective in the wet season. Pulice et al. (2013) also reported higher EC in samples collected after wet winter than in samples collected after dry winter.

Increase in leachate volume between treatments also brings scattering in cation and anion concentrations (**Figures 9C,D**). The low rainfall intensity treatments leached lower cation and anion concentrations. However, most of the dissimilarities occur in the freezing treatments. Canton et al. (2001) found different

trends of dissolved salt migration during drying periods which can be applied to wetting–drying processes investigated in this study. Not only volume but also total releases of cations and anions are higher in samples subjected to freezing, indicating the release and migration of dissolved salts. Drying at 50°C caused dissolved ions to migrate toward the surface and crystallize in the pores of sediments promoting fragmentation.

The similarity in both value and trend of total cation release among D, J, and X under every treatment indicates that chemical weathering has the same effect on D, J, and X. Significantly greater total cation release of A than the other three mudstone types, regardless of treatments, signifies that sample A is more susceptible to chemical leaching. The similarity in both the value and trend of total cation release between two levels of rainfall acidity shows that samples appear to be less sensitive to acidification.

The ratios between the leachate volume and pH, EC, and total releases of cations and anions show the equilibrium between stationary phase (i.e., sediment) and mobile phase (i.e., precipitation). During high-intensity rainfall, this equilibrium is moved toward desorption because sediment is releasing, that is, leaching anions. During low-intensity rainfall, there is a competition between ions from the rainfall and sediment for position on the sediment surface.

Based on the above discussion about the influence of each factor on physical disintegration, it can be summarized that under the conditions of temperature, intensity, and acidity of rain that can be achieved in nature, high rainfall and acid rain do increase the disintegration rates, but also high temperature definitely accelerates the rock disintegration by promoting the rate and magnitude of moisture variations (wetting and drying alterations). In addition to previous literature that emphasizes the strong influence of water over temperature (Sass, 2005; Doostmohammadi et al., 2008; Zhang et al., 2013), this finding confirms that impact and importance of the drying process caused by high temperature between wetting events need more attention. It is in accordance with the conclusion of Chen et al. (2021) that the temperature variations have similar influence on slope erosion as precipitation.

Nadal-Romero et al. (2022) indicate that in wet badlands weathering is controlled by freeze–thaw cycles, while wetting–drying cycles are the main weathering drivers in dry badlands with rainfall amount being the main driver for runoff generation. Our findings correspond to these findings with the addition of importance of drying between wetting events. Therefore, climatic variations of temperature can modify weathering processes, and in that way condition hydro-geomorphological processes in badland areas. Such changes should be considered for direct and indirect implications on badland dynamics, geomorphological processes, and on-site and off-site effects.

4 CONCLUSION

Based on the abovementioned discussion about the influences of each factor on mechanical disintegration and chemical leaching, it can be concluded that for the investigated sediments, under the conditions of temperature, intensity, and acidity of rain that can be achieved in nature,

1) high-drying temperature increases mechanical disintegration by promoting the rate and magnitude of moisture variations (wetting–drying alterations), while high rainfall intensity and acid rain have no obvious effect on physical disintegration. This conclusion confirms that impact and importance of the drying process caused by high temperature between wetting events on mechanical disintegration need more attention, rather than high rainfall intensity.
2) low temperature and high rainfall intensity causing larger total flux of water through the rock minerals and acid rain with higher concentration of H^+ in the water, contributing more H^+ required for cation exchanges, rock type with more soluble minerals, all promote chemical leaching. Also, the mineral composition of the rock has a greater effect on chemical leaching than climate conditions. The influence of climatic variables on chemical weathering decreases in the order as follows: high rainfall intensity > freezing temperature > acid rain.

DATA AVAILABILITY STATEMENT

The raw data supporting the conclusion of this article will be made available by the authors, without undue reservation.

AUTHOR CONTRIBUTIONS

XT and MK-G contributed to the conception and design of the study. CX, NA, EN-R, LY, TT, and SD participated in experiments. CX performed the analysis and wrote the first draft of the manuscript. All authors contributed to manuscript revision and read and approved the submitted version.

FUNDING

This study was supported by the National Natural Science Foundation of China (Grant Nos. 41771008, 51879288, and 41901005) and International Program for Ph.D. Candidates, Sun Yat-Sen University. The study and analyses were supported by the Ministry of Education, Science, and Technological Development, Republic of Serbia (Grant No. 451-03-68/2022-14/200026).

REFERENCES

Aly, N., Gomez–Heras, M., Hamed, A., Álvarez de Buergo, M., and Soliman, F. (2015). The Influence of Temperature in a Capillary Imbibition Salt Weathering Simulation Test on Mokattam Limestone. *Mat. Construcc.* 65 (317), e044. doi:10.3989/mc.2015.00514

Bruthans, J., Filippi, M., Schweigstillová, J., and Řihošek, J. (2017). Quantitative Study of a Rapidly Weathering Overhang Developed in an Artificially Wetted Sandstone Cliff. *Earth Surf. Process. Landforms* 42, 711–723. doi:10.1002/esp.4016

Bubeck, A., Walker, R. J., Healy, D., Dobbs, M., and Holwell, D. A. (2017). Pore Geometry as a Control on Rock Strength. *Earth Planet. Sci. Lett.* 457, 38–48. doi:10.1016/j.epsl.2016.09.050

Cantón, Y., Solé-Benet, A., Queralt, I., and Pini, R. (2001). Weathering of a Gypsum-Calcareous Mudstone under Semi-arid Environment at Tabernas, SE Spain: Laboratory and Field-Based Experimental Approaches. *Catena* 44, 111–132. doi:10.1016/S0341-8162(00)00153-3

Chen, Z., Yan, L., Peng, H., and Shi, H. (2021). Temperature Controls on the Erosion of Badland Slopes in the Nanxiong Basin, China. *Front. Earth Sci.* 9, 712134. doi:10.3389/feart.2021.712134

Chigira, M., and Oyama, T. (2000). Mechanism and Effect of Chemical Weathering of Sedimentary Rocks. *Eng. Geol.* 55, 3–14. doi:10.1016/S0013-7952(99)00102-7

Colback, P., and Wiid, B. L. (1965). The Influence of Moisture Content on the Compressive Strength of Rocks. *Proc.rock Mech.symp.tronto*, 84, 65–83.

Doostmohammadi, R., Moosavi, M., Mutschler, T., and Osan, C. (2008). Influence of Cyclic Wetting and Drying on Swelling Behavior of Mudstone in South West of Iran. *Environ. Geol.* 58, 999–1009. doi:10.1007/s00254-008-1579-3

Egli, M., Mirabella, A., Sartori, G., and Fitze, P. (2003). Weathering Rates as a Function of Climate: Results from a Climosequence of the Val Genova (Trentino, Italian Alps). *Geoderma* 111, 99–121. doi:10.1016/S0016-7061(02)00256-2

Egli, M., Mirabella, A., and Sartori, G. (2008). The Role of Climate and Vegetation in Weathering and Clay Mineral Formation in Late Quaternary Soils of the Swiss and Italian Alps. *Geomorphology* 102, 307–324. doi:10.1016/j.geomorph.2008.04.001

Erguler, Z. A., and Shakoor, A. (2009). Relative Contribution of Various Climatic Processes in Disintegration of Clay-Bearing Rocks. *Eng. Geol.* 108, 36–42. doi:10.1016/j.enggeo.2009.06.002

Gallart, F., Pérez-Gallego, N., Latron, J., Catari, G., Martínez-Carreras, N., and Nord, G. (2013). Short- and Long-Term Studies of Sediment Dynamics in a Small Humid Mountain Mediterranean Basin with Badlands. *Geomorphology* 196, 242–251. doi:10.1016/j.geomorph.2012.05.028

Gallart, F., Solé, A., Puigdefábregas, J., and Lázaro, R. (2002). "Badland Systems in the Mediterranean," in *Dryland Rivers: Hydrology and Geomorphology of Semi-arid Channels*. Editors L. J. Bull and M. J. Kirkby (Chichester, London: John Wiley & sons Press), 299–326.

Ghobadi, M. H., and Torabi-Kaveh, M. (2014). Assessing the Potential for Deterioration of Limestones Forming Taq-E Bostan Monuments under Freeze-Thaw Weathering and Karst Development. *Environ. Earth Sci.* 72, 5035–5047. doi:10.1007/s12665-014-3373-8

Goudie, A. S., and Viles, H. A. (2012). Weathering and the Global Carbon Cycle: Geomorphological Perspectives. *Earth-Science Rev.* 113, 59–71. doi:10.1016/j.earscirev.2012.03.005

G. R. L., and ., M. B. (2002). The Role of Mineralogy on Durability of Weak Rocks. *J. Appl. Sci.* 2, 698–701. doi:10.3923/jas.2002.698.701

Gupta, V., and Ahmed, I. (2007). The Effect of pH of Water and Mineralogical Properties on the Slake Durability (Degradability) of Different Rocks from the Lesser Himalaya, India. *Eng. Geol.* 95, 79–87. doi:10.1016/j.enggeo.2007.09.004

Hale, P. A., and Shakoor, A. (2003). A Laboratory Investigation of the Effects of Cyclic Heating and Cooling, Wetting and Drying, and Freezing and Thawing on the Compressive Strength of Selected Sandstones. *Environ. Eng. Geoscience* 9, 117–130. doi:10.2113/9.2.117

Hall, K. (2007). Evidence for Freeze-Thaw Events and Their Implications for Rock Weathering in Northern Canada: II. The Temperature at Which Water Freezes in Rock. *Earth Surf. Process. Landforms* 32, 249–259. doi:10.1002/esp.1389

Hall, K., and Hall, A. (1991). Thermal Gradients and Rock Weathering at Low Temperatures: Some Simulation Data. *Permafr. Periglac. Process.* 2, 103–112. doi:10.1002/ppp.3430020205

Heap, M. J., Xu, T., and Chen, C.-f. (2014). The Influence of Porosity and Vesicle Size on the Brittle Strength of Volcanic Rocks and Magma. *Bull. Volcanol.* 76. doi:10.1007/s00445-014-0856-0

Huang, J., and Xie, P. (2015). Analysis of Acid Rain in Shaoguan City Present Situation and Prevention Measures. *Guangdong Chem. Ind.* 42, 184–185. doi:10.5814/j.issn.1674-764x.2021.05.002

Kasanin-Grubin, M., and Bryan, R. (2007). Lithological Properties and Weathering Response on Badland Hillslopes. *Catena* 70 (1), 68–78. doi:10.1016/j.catena.2006.08.001

Kasanin-Grubin, M. (2013). Clay Mineralogy as a Crucial Factor in Badland Hillslope Processes. *Catena* 106, 54–67. doi:10.1016/j.catena.2012.08.008

Li, D., Wang, G., Han, L. Q., Liu, P. Y., He, M. C., Yang, G. X., et al. (2011). Analysis of Microscopic Pore Structures of Rocks Before and After Water Absorption. *Int. J. Min. Sci. Technol.* 21, 287–293. doi:10.1016/j.mstc.2011.02.002

Li, Z., Xu, G., Zhao, X., Fu, Y., and Su, C. (2019). Experimental Study on Water Absorption and Weakening of Silurian Argillite. *Geotech. Geol. Eng.* 37, 3881–3890. doi:10.1007/s10706-019-00878-1

Likens, G. E., Driscoll, C. T., and Buso, D. C. (1996). Long-Term Effects of Acid Rain: Response and Recovery of a Forest Ecosystem. *Science* 272, 244–246. doi:10.1126/science.272.5259.244

Lu, H., Yu, P., Yan, J. P., Shao, D. Y., Jia, X. J., and Zhang, W. T. (2015). Experimental Investigation of Water Absorption and its Significance on Pore Network Connectivity in Mudstone from Silurian Longmaxi Formation, Sichuan Basin. *Nat. Gas. Geosci.* 26, 1556–1562. doi:10.11764/j.issn.1672-1926.2015.08.1556

Migoń, P. (2013). "Weathering and Hillslope Development," in *Treatise on Geomorphology*. Editor J. F. Shroder (San Diego: Academic Press), 159–178. doi:10.1007/3-540-31060-6_405

Nadal-Romero, E., and Regüés, D. (2010). Geomorphological Dynamics of Subhumid Mountain Badland Areas - Weathering, Hydrological and Suspended Sediment Transport Processes: A Case Study in the Araguás Catchment (Central Pyrenees) and Implications for Altered Hydroclimatic Regimes. *Prog. Phys. Geogr. Earth Environ.* 34 (2), 123–150. doi:10.1177/0309133309356624

Nadal-Romero, E., Revuelto, J., Errea, P., and López-Moreno, J. I. (2015). The Application of Terrestrial Laser Scanner and SfM Photogrammetry in Measuring Erosion and Deposition Processes in Two Opposite Slopes in a Humid Badlands Area (Central Spanish Pyrenees). *SOIL* 1 (2), 561–573. doi:10.5194/soil-1-561-2015

Nadal-Romero, E., Rodriguez-Caballero, E., Chamizo, S., Juez, C., Canton, Y., and Garcia-Ruiz, J. M. (2022). Mediterranean Badlands: Their Driving Processes and Climate Futures. *Earth Surf. Process. Landforms* 47, 17–31. doi:10.1002/esp.5088

Ondrášik, M., and Kopecký, M. (2014). Rock Pore Structure as Main Reason of Rock Deterioration. *Studia Geotechnica Mech.* 36, 79–88. doi:10.2478/sgem-2014-0010

Pejon, O. J., and Zuquette, L. V. (2002). Analysis of Cyclic Swelling of Mudrocks. *Eng. Geol.* 67, 97–108. doi:10.1016/s0013-7952(02)00147-3

Piccarreta, M., Faulkner, H., Bentivenga, M., and Capolongo, D. (2006). The Influence of Physico-Chemical Material Properties on Erosion Processes in the Badlands of Basilicata, Southern Italy. *Geomorphology* 81, 235–251. doi:10.1016/j.geomorph.2006.04.010

Pulice, I., Di Leo, P., Robustelli, G., Scarciglia, F., Cavalcante, F., and Belviso, C. (2013). Control of Climate and Local Topography on Dynamic Evolution of Badland from Southern Italy (Calabria). *Catena* 109, 83–95. doi:10.1016/j.catena.2013.05.001

Regüés, D., Guàrdia, R., and Gallart, F. (2000). Geomorphic Agents versus Vegetation Spreading as Causes of Badland Occurrence in a Mediterranean Subhumid Mountainous Area. *Catena* 40, 173–187. doi:10.1016/S0341-8162(99)00045-4

Robinson, D. A., and Phillips, C. P. (2001). Crust Development in Relation to Vegetation and Agricultural Practice on Erosion Susceptible, Dispersive Clay Soils from Central and Southern Italy. *Soil Tillage Res.* 60, 1–9. doi:10.1016/S0167-1987(01)00166-0

Robinson, D. A., and Williams, R. B. G. (2000). Experimental Weathering of Sandstone by Combinations of Salts. *Earth Surf. Process. Landforms* 25, 1309–1315. doi:10.1002/1096-9837(200011)25:12<1309::aid-esp139>3.0.co;2-5

Sass, O. (2005). Rock Moisture Measurements: Techniques, Results, and Implications for Weathering. *Earth Surf. Process. Landforms* 30, 359–374. doi:10.1002/esp.1214

Slavík, M., Bruthans, J., Weiss, T., and Schweigstillová, J. (2020). Measurements and Calculations of Seasonal Evaporation Rate from Bare Sandstone Surfaces: Implications for Rock Weathering. *Earth Surf. Process. Landforms* 45, 2965–2981. doi:10.1002/esp.4943

Spatti Júnior, E. P., da Conceição, F. T., Fernandes, A. M., Sardinha, D. d. S., Menegário, A. A., and Moruzzi, R. B. (2019). Chemical Weathering Rates of Clastic Sedimentary Rocks from the Paraná Basin in the Paulista Peripheral Depression, Brazil. *J. S. Am. Earth Sci.* 96, 102369. doi:10.1016/j.jsames.2019.102369

Summa, V., Tateo, F., Medici, L., and Giannossi, M. L. (2007). The Role of Mineralogy, Geochemistry and Grain Size in Badland Development in Pisticci (Basilicata, Southern Italy). *Earth Surf. Process. Landforms* 32, 980–997. doi:10.1002/esp.1449

Sverdrup, H., and Warfvinge, P. (1990). The Role of Weathering and Forestry in Determining the Acidity of Lakes in Sweden. *Water Air Soil Pollut.* 52, 71–78. doi:10.1007/BF00283115

Turkington, A. V., and Paradise, T. R. (2005). Sandstone Weathering: a Century of Research and Innovation. *Geomorphology* 67, 229–253. doi:10.1016/j.geomorph.2004.09.028

Vet, R., Artz, R. S., Carou, S., Shaw, M., Ro, C.-U., Aas, W., et al. (2014). A Global Assessment of Precipitation Chemistry and Deposition of Sulfur, Nitrogen, Sea Salt, Base Cations, Organic Acids, Acidity and pH, and Phosphorus. *Atmos. Environ.* 93, 3–100. doi:10.1016/j.atmosenv.2013.10.060

Viles, H. A. (2013). Linking Weathering and Rock Slope Instability: Non-linear Perspectives. *Earth Surf. Process. Landforms* 38, 62–70. doi:10.1002/esp.3294

Wang, S., Han, L., Meng, Q., Jin, Y., and Zhao, W. (2019a). Investigation of Pore Structure and Water Imbibition Behavior of Weakly Cemented Silty Mudstone. *Adv. Civ. Eng.* 2019, 1–13. doi:10.1155/2019/8360924

Wang, S., Han, L., Meng, Q., Jin, Y., and Zhao, W. (2019b). Water Absorption/dehydration by NMR and Mechanical Response for Weakly Cemented Mudstones Subjected to Different Humidity Conditions. *Bull. Eng. Geol. Environ.* 79, 1275–1288. doi:10.1007/s10064-019-01629-5

Warke, P. A., and Smith, B. J. (1998). Effects of Direct and Indirect Heating on the Validity of Rock Weathering Simulation Studies and Durability Tests. *Geomorphology* 22, 347–357. doi:10.1016/S0169-555X(97)00078-0

Weiss, T., Siegesmund, S., Kirchner, D., and Sippel, J. (2004). Insolation Weathering and Hygric Dilatation: Two Competitive Factors in Stone Degradation. *Env. Geol.* 46 (3), 402–413. doi:10.1007/s00254-004-1041-0

White, A. F., and Blum, A. E. (1995). Effects of Climate on Chemical_ Weathering in Watersheds. *Geochimica Cosmochimica Acta* 59, 1729–1747. doi:10.1016/0016-7037(95)00078-E

Wilson, M. J. (2004). Weathering of the Primary Rock-Forming Minerals: Processes, Products and Rates. *Clay Min.* 39, 233–266. doi:10.1180/0009855043930133

Yamaguchi, H., Yoshida, K., Kuroshirna, I., and Fukuda, M. (1988). Slaking and Shear Properties of Mudstone. *ISRM Int. Symp.* 1988, 133–144. doi:10.1016/0148-9062(89)92095-0

Yan, L., Liu, P., Peng, H., Kašanin-Grubin, M., and Lin, K. (2018). Laboratory Study of the Effect of Temperature Difference on the Disintegration of Redbed Softrock. *Phys. Geogr.* 40, 149–163. doi:10.1080/02723646.2018.1559418

Yang, Y., and Aplin, A. C. (2010). A Permeability-Porosity Relationship for Mudstones. *Mar. Petroleum Geol.* 27, 1692–1697. doi:10.1016/j.marpetgeo.2009.07.001

Zhang, D., Chen, A., Wang, X., and Liu, G. (2015). Quantitative Determination of the Effect of Temperature on Mudstone Decay during Wet-Dry Cycles: A Case Study of 'purple Mudstone' from South-Western China. *Geomorphology* 246, 1–6. doi:10.1016/j.geomorph.2015.06.011

Zhang, D., Chen, A., Wang, X., Yan, B., Shi, L., and Liu, G. (2016). A Quantitative Determination of the Effect of Moisture on Purple Mudstone Decay in Southwestern China. *Catena* 139, 28–31. doi:10.1016/j.catena.2015.12.003

Zhang, D., Chen, A., Xiong, D., and Liu, G. (2013). Effect of Moisture and Temperature Conditions on the Decay Rate of a Purple Mudstone in Southwestern China. *Geomorphology* 182, 125–132. doi:10.1016/j.geomorph.2012.11.003

Zhao, J., Lu, C., Deng, L., and Liu, G. (2018). Impacts of Simulated Acid Solution on the Disintegration and Cation Release of Purple Rock (Mudstone) in Southwest China. *Geomorphology* 316, 35–43. doi:10.1016/j.geomorph.2018.05.009

Conflict of Interest: The authors declare that the research was conducted in the absence of any commercial or financial relationships that could be construed as a potential conflict of interest.